catalysts

MDPI

Article

Pd/Fe_3O_4 Nanofibers for the Catalytic Conversion of Lignin-Derived Benzyl Phenyl Ether under Transfer Hydrogenolysis Conditions

Angela Malara [1,*], Emilia Paone [2], Lucio Bonaccorsi [1], Francesco Mauriello [1], Anastasia Macario [3] and Patrizia Frontera [1]

1 Dipartimento DICEAM, Università Mediterranea di Reggio Calabria, Loc. Feo di Vito, I-89122 Reggio Calabria, Italy; lucio.bonaccorsi@unirc.it (L.B.); francesco.mauriello@unirc.it (F.M.); patrizia.frontera@unirc.it (P.F.)

2 Dipartimento di Ingegneria Industriale, Università degli Studi di Firenze, Via Santa Marta 3, 50139 Firenze, Italy; emilia.paone@unirc.it

3 Dipartimento di Ingegneria per l'Ambiente e il Territorio e Ingegneria Chimica, Università della Calabria, Via P. Bucci, Arcavacata di Rende, I-87036 Cosenza, Italy; anastasia.macario@unirc.it

* Correspondence: angela.malara@unirc.it

Received: 14 November 2019; Accepted: 19 December 2019; Published: 22 December 2019

Abstract: Novel magnetite-supported palladium catalysts, in the form of nanofiber materials, were prepared by using the electrospinning process. Two different synthetic techniques were used to add palladium to the nanofibers: (i) the wet impregnation of palladium on the Fe_3O_4 electrospun support forming the Pd/Fe_3O_4[wnf] catalyst or (ii) the direct co-electrospinning of a solution containing both metal precursor specimens leading to a Pd/Fe_3O_4[cnf] sample. The obtained Pd-based Fe_3O_4 nanofibers were tested in the transfer hydrogenolysis of benzyl phenyl ether (BPE), one of the simplest lignin-derived aromatic ethers, by using 2-propanol as H-donor/solvent, and their performances were compared with the analogous impregnated Pd/Fe_3O_4 catalyst and a commercial Pd/C. A morphological and structural characterization of the investigated catalysts was performed by means of SEM-EDX, TGA-DSC, XRD, TEM, H_2-TPR, and N_2 isotherm at 77 K analysis. Pd/Fe_3O_4[wnf] was found to be the best catalytic system allowing a complete BPE conversion after 360 min at 240 °C and a good reusability in up to six consecutive recycling tests.

Keywords: electrospinning; heterogeneous catalysis; palladium; iron oxide; transfer hydrogenolysis; benzyl phenyl ether; lignin; aromatic ethers

1. Introduction

In the last several decades, thanks to all opportunities offered by nanotechnology and nanoscience, a huge advance in the preparation methods of heterogeneous supported catalysts (impregnation, precipitation/co-precipitation, chemical vapor deposition, grafting, etc.) has been observed [1–3]. A great deal of attention has been paid to the development of synthetic procedures that can opportunely tune the textural properties of materials, thus driving their catalytic performances [1–3].

In this context, one-dimensional (1D) nanocatalysts have recently gained consideration [4–6], highlighting how nanofibrous supports can improve the metal dispersion, thus allowing an increase of the surface area-to-volume ratio that enhances the catalytic performance [7,8]. Among several methods adopted for producing 1D nanomaterials, the electrospinning technique can be successfully used to produce submicron fibers in a simple and feasible process [9–16].

In the electrospinning process, a precursor polymer solution, eventually containing the precursor of inorganic phases, is pumped by a capillary pump and charged by a supplied high voltage. The

charged composite blend polymer jet undergoes stretching before it reaches the collector and, after the evaporation of the solvent, solidifies in nanofibers form. Then, the obtained composite is calcined at a prefixed temperature to obtain pure inorganic phase nanofibers. Indeed, the electrospun fibers show excellent features such as nanosize, mesoporous nanostructure, large specific surface area, and controllable morphology. These features make the nanofibers a promising and attractive candidate for catalyst support because they can provide more active sites for the catalyst, thus improving the catalytic efficiency [5]. Moreover, the electrospinning technique offers a simple and versatile route to immobilize metal particles in submicron-sized fibers improving the operational stability of samples when used, for example, in plug-flow reactors.

Recently different nanofibers have been proposed for different catalytic applications [17]. For example, an electrospun nanofiber NiO catalyst was tested in the transfer hydrogenation of aromatic aldehydes and hydration of aromatic nitriles and was highly catalytically efficient, with a yield of above 90% [18]. A supported catalyst in the form of a Cu-doped cerium oxide nanofiber sample was prepared by electrospinning, obtaining a fiber-like nanostructure with higher surface area and higher Cu^{2+} dispersion compared with a particle-like catalyst [8].

In this study, two novel Pd/Fe_3O_4 nanofiber-based catalysts were prepared via electrospinning by using two different synthetic approaches (Scheme 1):

- The impregnation of calcined iron(III) oxide electrospun nanofibers with a solution of a Pd(II) precursor followed by H_2 reduction (Pd/Fe_3O_4[wnf] catalyst).
- The direct co-electrospinning of the two solutions containing the metal solutions of the corresponding inorganic Pd^{2+} and Fe^{3+} precursors followed by calcination and H_2 reduction (Pd/Fe_3O_4[cnf] catalyst).

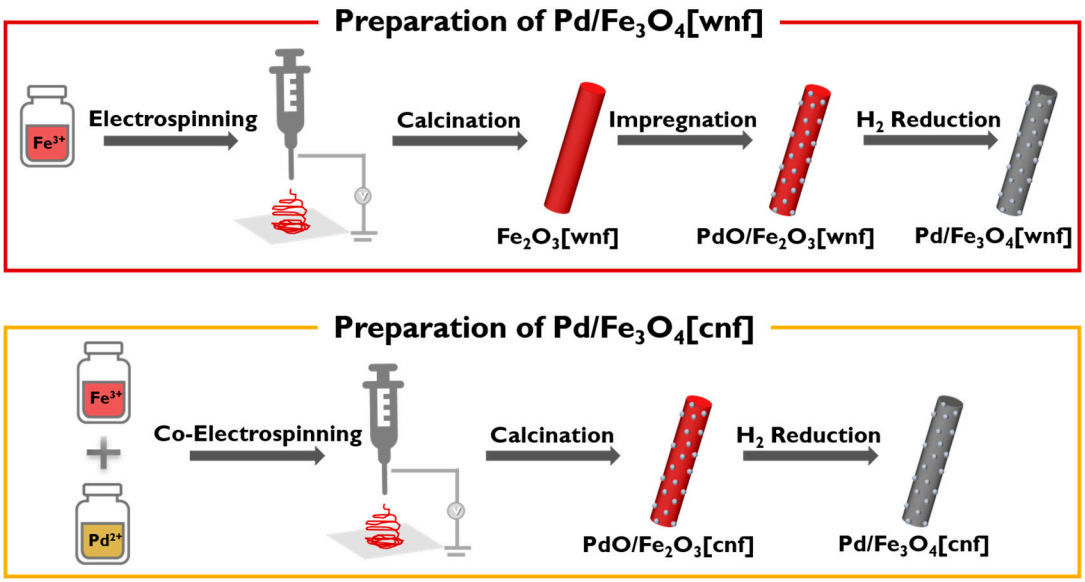

Scheme 1. Schematic procedures for the preparation of Pd/Fe_3O_4[wnf] and Pd/Fe_3O_4[cnf] nanofiber catalysts.

This type of heterogeneous Pd/Fe_3O_4 catalyst has been successfully used in the cleavage of C–O and C–C bonds of lignocellulosic derived molecules under catalytic transfer hydrogenolysis (CTH) conditions [19–21]. In CTH reactions, the use of an indirect H source such as 2-propanol, ethanol, methanol, or formic acid allows the lysis of carbon–carbon or carbon–heteroatom bonds in lignocellulosic biomasses and in their derived model molecules, thus lowering their oxygen content [22–24]. At the same time, under CTH conditions, it is possible to reduce problems related to the direct use of molecular hydrogen (purchase, transport, security hazards, expensive infrastructures, etc.).

The catalysts were tested in the transfer hydrogenolysis of benzyl phenyl ether (BPE), which is one of the simplest lignin-derived aromatic ethers, generally used as model molecule to mimic the catalytic cleavage of α-O-4 lignin linkages (Scheme 2) [25–27]. Lignin is the only fraction of lignocellulosic biomasses that, via catalytic depolymerization, is suitable for the sustainable production of aromatic compounds. Thus, it has attracted a great deal of attention in recent years [28,29]. The catalyst activity is decisive both in the reductive cleavage of C–C and C–O bonds, as well as in the stabilization of the lignin fragments [30–32]. Among the most adopted catalytic systems, Pd-based catalysts are surely among the most investigated [33–37].

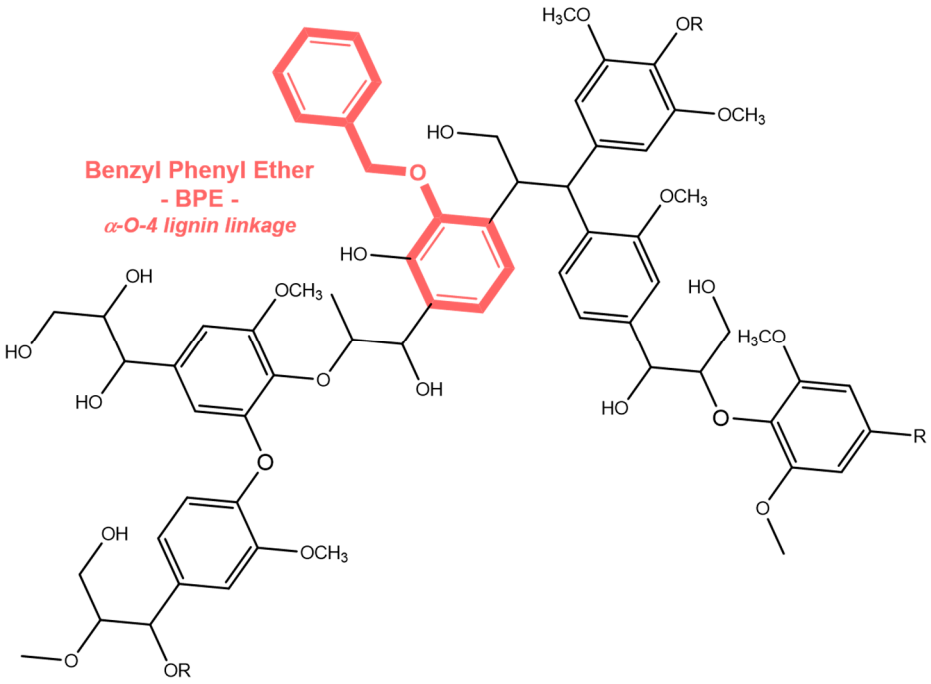

Scheme 2. Benzyl phenyl ether (BPE) as model molecule that mimic the catalytic cleavage of α-O-4 lignin linkages.

2. Results and Discussion

2.1. Catalyst Characterization

Having the aim of obtaining a fibrous morphology, a key parameter in the electrospinning process is generally the viscosity of the spinnable solution. For both Pd/Fe_3O_4[wnf] and Pd/Fe_3O_4[cnf] systems, the optimal conditions to achieve a suitable viscosity (around 1.30–1.40 Pa at 25 °C) were identified. Moreover, after a number of experiments, the formation of the "Taylor cone" was finally realized at the optimized flow rate of 1.41 mL/h, high voltage of 17 kV, and needle-to-collector distance of 12 cm.

The SEM images of the as spun composite nanofibers showed a smooth surface (Figure 1), with an average diameter of around 450 nm for the electrospun support $Fe(OH)_x$[nf] and for the co-electrospun $PdO/Fe(OH)_x$[cnf] sample, highlighting that the presence of palladium in the precursor solution did not affect the nanofiber diameters.

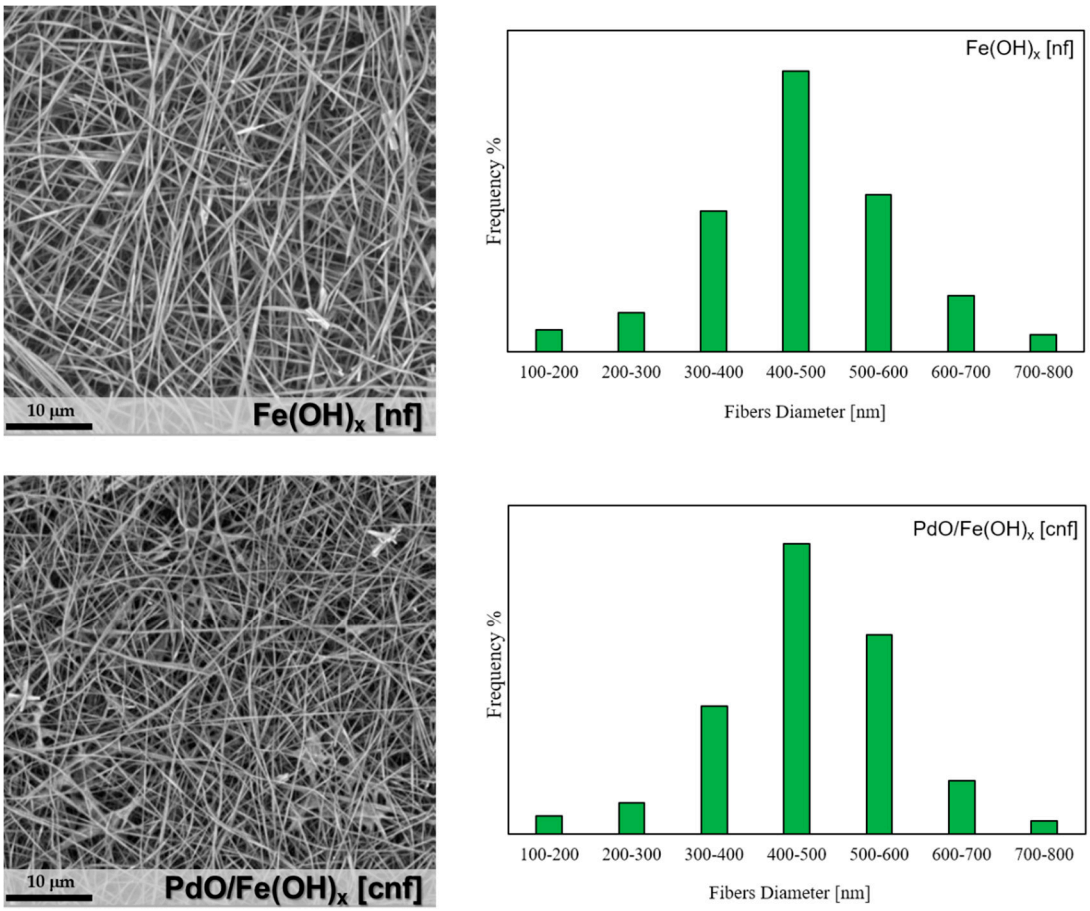

Figure 1. SEM images of as-spun $Fe(OH)_x$[nf] and $PdO/Fe(OH)_x$[cnf] samples, together with their fibers diameter distribution.

The electrospun nanofibers were composed of organic polymer and ceramic and/or metallic precursor compounds. In order to remove the polymer, the as-spun fibers needed to be calcined. The calcination temperature was determined according to the thermal gravimetric analysis (TGA) of the polymer polyacrylonitrile (PAN) used in the precursor solution for electrospinning (Figure 2). PAN degraded completely below 500 °C [38], as shown by the thermal analysis results carried out on both samples, PdO/Fe_2O_3[wnf] and PdO/Fe_2O_3[cnf] (Figure 2). Moreover, the different catalyst preparation methods did not affect the thermal profiles, since both catalysts exhibited the relevant weight loss in the range 200–450 °C, attributable to polymer degradation.

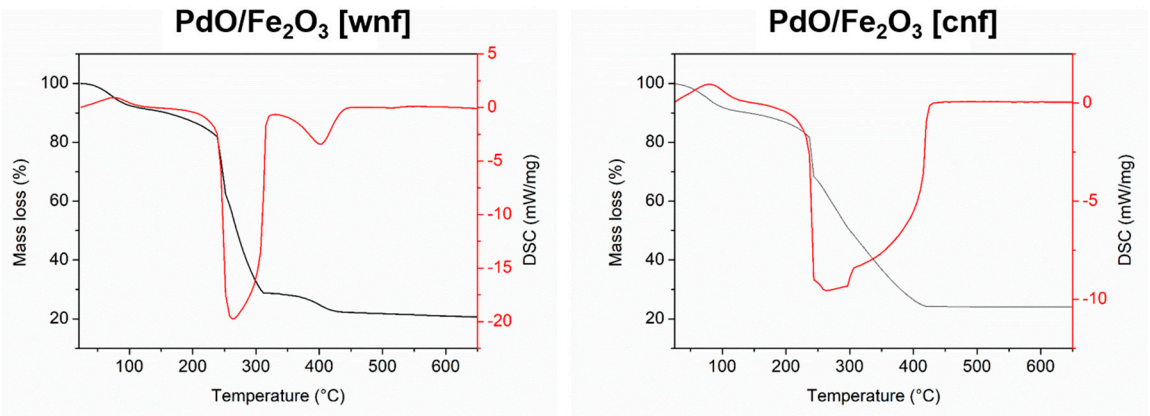

Figure 2. TGA and DSC profiles of PdO/Fe_2O_3[wnf] and PdO/Fe_2O_3[cnf] samples.

Similarly, a comparative evaluation of specific surface areas obtained using Brunauer–Emmett–Teller (BET) equation applied to the N_2 adsorption–desorption isotherms at 77 K, on both electrospun samples, confirmed that there were no changes as a result of the different synthesis methods. The calculated specific surface areas of the analyzed samples are shown in Table 1.

Table 1. Main characteristics of the supported palladium catalysts investigated (S.A.: surface area; d_n: mean particle size from TEM).

Samples	Palladium Loading (wt%)	Catalyst Preparation	S.A. (m^2/g)	d_n (nm)
Pd/Fe_3O_4[wnf]	4.3	Impregnation of Fe_2O_3 nanofibers	234	10.5
Pd/Fe_3O_4[cnf]	3.7	Co-electrospinning	228	8.5
Pd/Fe_3O_4	5.2	Impregnation of commercial Fe_3O_4	60	8.8
Pd/C	5.0	Commercial	600	10.2

The TPR-H_2 profiles of calcined samples, PdO/Fe_2O_3[wnf] and PdO/Fe_2O_3[cnf], are reported in Figure 3. In both cases, the first peak belongs to the palladium specimen reduction, whereas the higher-temperature peaks can be assigned to the Fe_3O_4 support reduction, slightly shifted towards lower temperatures with respect to the peak of the corresponding pure oxides, suggesting a metal–support interaction [39–42].

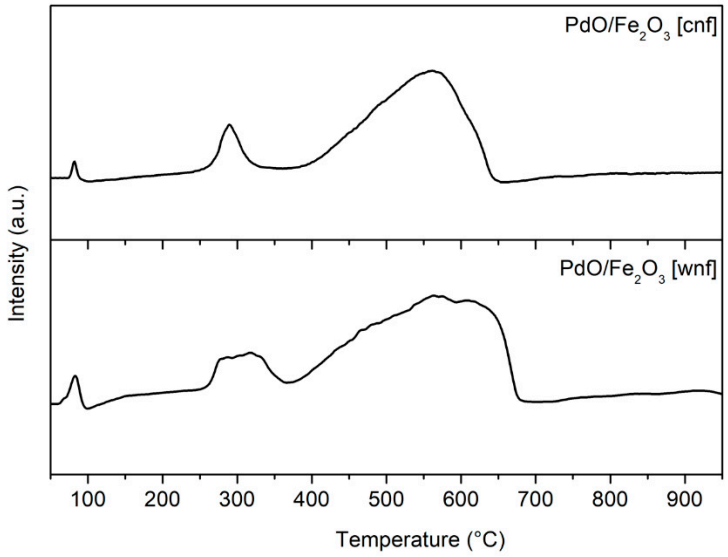

Figure 3. The H_2-TPR profiles of PdO/Fe_2O_3[wnf] and PdO/Fe_2O_3[cnf] samples.

In the XRD patterns of the calcined samples (Figure 4), sharp peaks corresponding to the Fe_2O_3 phase were noticed (JCPDS card no. 33-0664). After the reduction under hydrogen flow, both samples showed the peaks related to the Fe_3O_4 phase (JCPDS card no. 19-0629). The absence of the (111) diffraction line of metallic palladium is indicative of extremely small highly dispersed Pd particles [22,43].

This was also confirmed by TEM results (Figure 5). For both reduced samples, the smooth composite nanofibers turned into rough nanofibers. Furthermore, the average nanofiber diameter decreased since the diameter of single nanofibers shrank down by about four times in both samples. According to TEM measurements (Figure 5), the catalyst sample Pd/Fe_3O_4[wnf] was composed of iron oxide grains decorated with palladium nanoparticles, having a mean diameter of 10 nm. For the catalytic sample obtained by co-electrospinning of Pd/Fe_3O_4[cnf], the metallic palladium particles still exhibited nanometric dimensions (mean diameter dimension: 9 nm) but also appeared to be embedded within the oxide fibers, which in turn seemed less wrinkled.

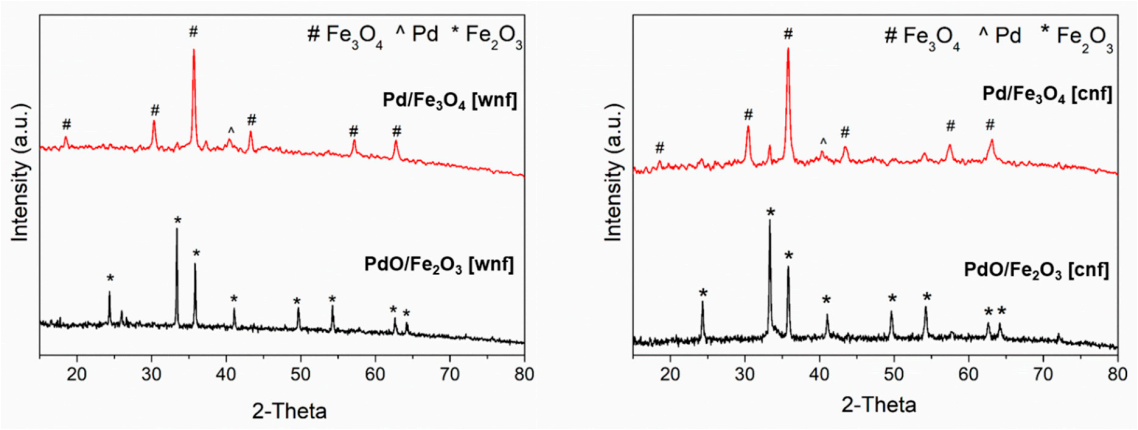

Figure 4. XRD spectra of investigated Pd-based iron oxide nanofiber catalysts.

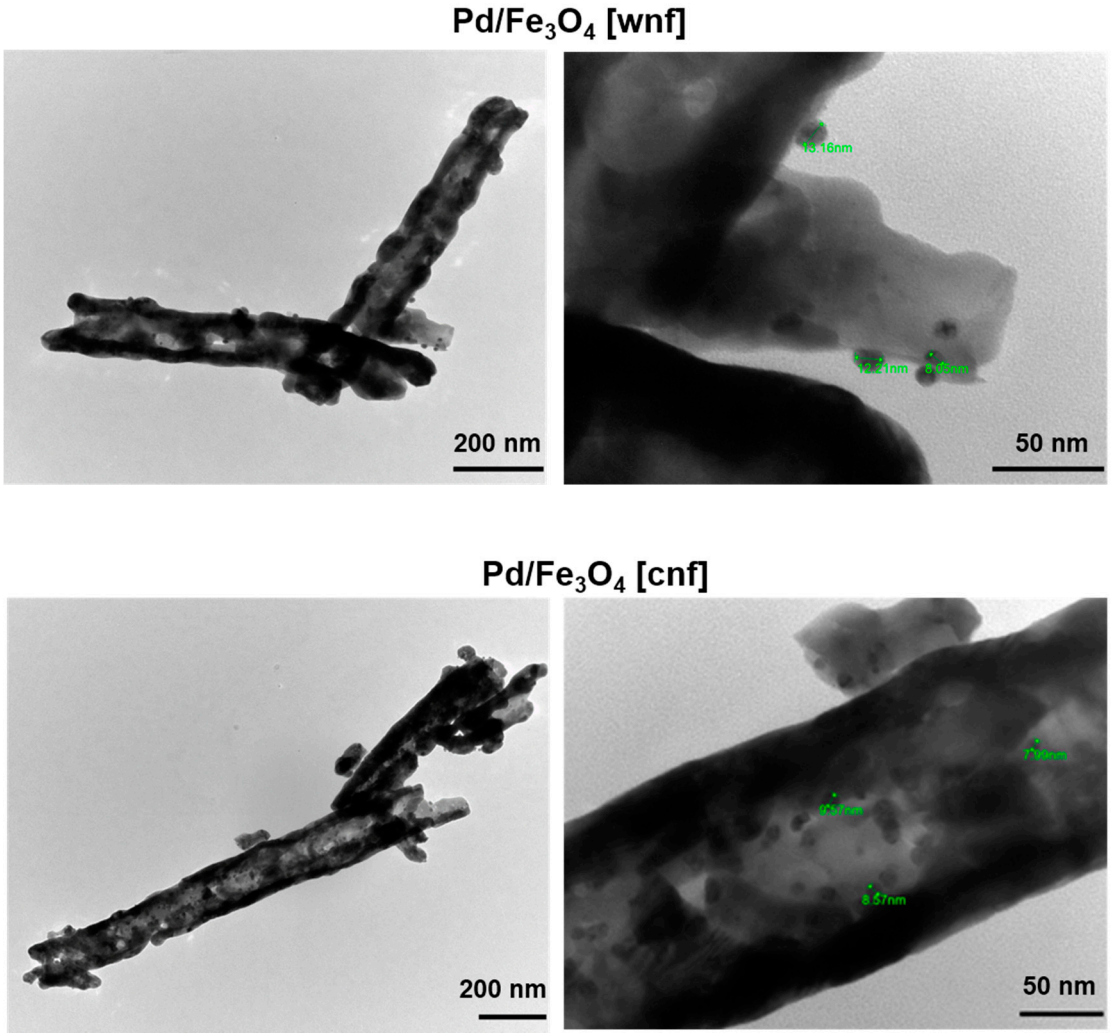

Figure 5. TEM images of samples Pd/Fe_3O_4[wnf] and Pd/Fe_3O_4[cnf] and relative Pd particle size dimensions.

The homogeneous distribution of palladium in the reduced samples, co-electrospun Pd/Fe_3O_4[cnf] and impregnated Pd/Fe_3O_4[wnf], was also confirmed by EDX color mapping (Figure 6). EDX spectra indicate a Pd/Fe_3O_4 ratio in close agreement with the 5:95 ratio considered in the electrospinning precursor solution.

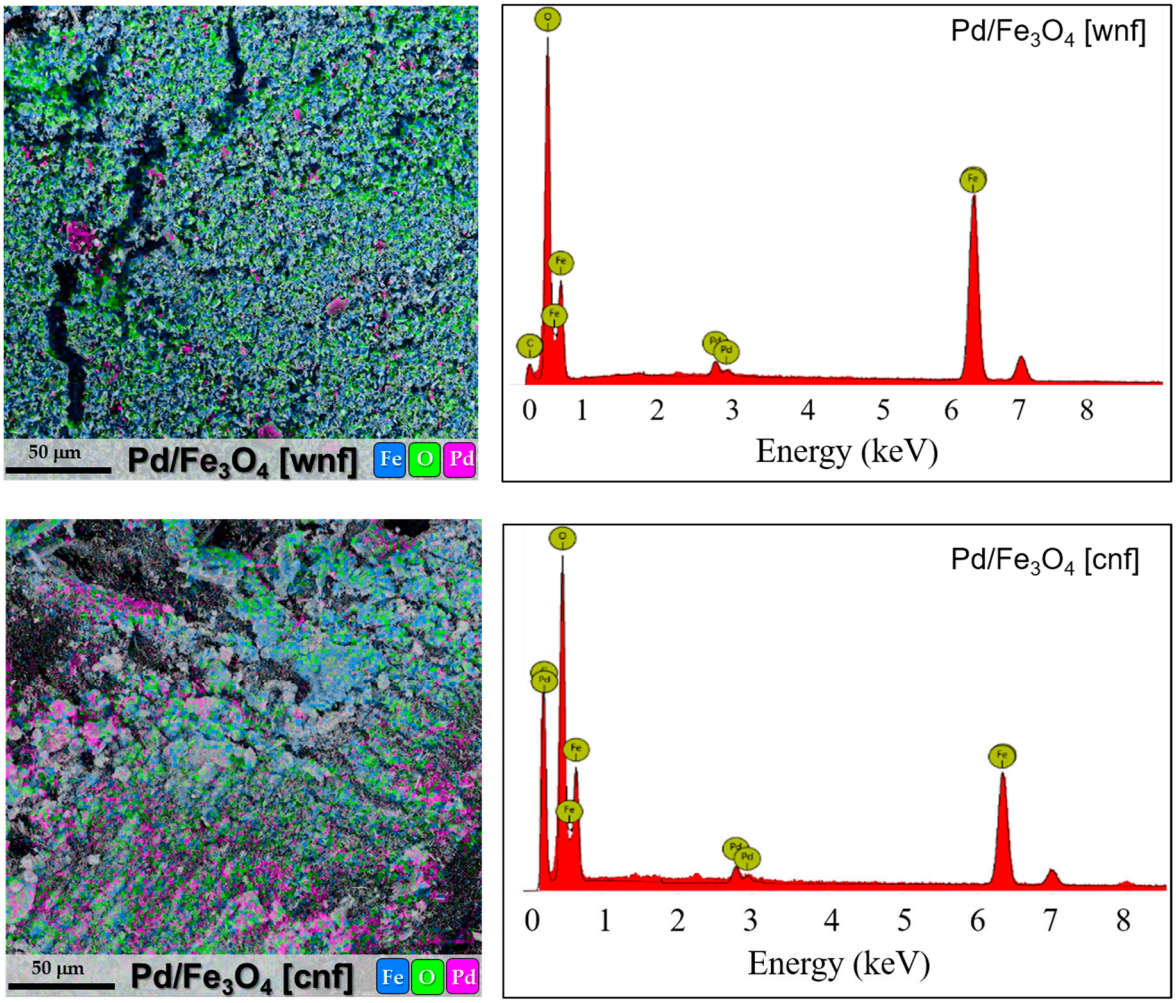

Figure 6. EDX spectra and colored maps of Pd/Fe_3O_4[wnf] and Pd/Fe_3O_4[cnf] samples.

A more detailed physicochemical characterization of both Pd/Fe_3O_4[wnf] and Pd/Fe_3O_4[cnf] catalytic systems, including ICP-MS, is currently in progress and will be object of future contributions.

2.2. Catalytic Tests

Table 2 reports the catalytic results of investigated catalysts in the CTH of BPE at 240 °C after 90 min of reaction time.

Table 2. Performance of investigated Pd-based catalysts in the transfer hydrogenolysis of benzyl phenyl ether (BPE) in the presence of 2-propanol as solvent/H-source (reaction conditions: 0.125 g of catalyst; 40 mL 0.1 M BPE solution; time, 90 min; N_2 pressure, 10 bar; stirring, 500 rpm).

Entry	Catalyst	Temperature (°C)	Conversion (%)	Aromatic Selectivity (%)
1	Pd/Fe_3O_4[wnf]	240	59	100
2	Pd/Fe_3O_4[cnf]	240	21	100
3	Pd/Fe_3O_4	240	38	100
4	Pd/C	240	8	100

By using Pd/Fe_3O_4[wnf], a good BPE conversion (60%) was registered, with toluene (TOL) and phenol (PHE) being the only reaction products observed. On the other hand, Pd/Fe_3O_4[cnf], impregnated Pd/Fe_3O_4 and commercial Pd/C—used as benchmark catalysts—exhibited a lower activity.

On the other hand, in the past, coprecipitated Pd/Fe_3O_4 catalyst showed a complete BPE conversion under analogous CTH reaction conditions (0.25 g of catalyst; 60 mL of entry solution; 240 °C; 10 bar N_2; 90 min) [25]. However, with all the investigated catalysts, reaction products derived from aromatic ring hydrogenation were not detected.

Results of reactions carried out at 240 °C allow us to discriminate which is the most important factor in the CTH of BPE. The pure Fe_3O_4 support (in the form of either commercial powder or nanofibers) did not give any BPE conversion, suggesting that Pd sites are an essential prerequisite for the CTH process. At the same time, Pd/C, with a specific surface area of 600 m^2/g, was found to be poorly active, clearly indicating that the performance of Pd-based catalysts cannot be attributed to any surface area effect. Reasonably, the higher performance of the Pd/Fe_3O_4[wnf] catalyst can be attributed to a strong metal support interaction, as revealed by H_2-TPR analysis and in agreement with a recent report on analogous heterogeneous Pd/Fe catalytic systems on the CTH of lignin-derived aromatic ethers [19]. On the other hand, the lower activity shown by Pd/Fe_3O_4[cnf] can be explained on the basis of TEM analysis results. Indeed, our experiments highlight that palladium particles were embedded inside the iron oxide nanofibers, thus decreasing the availability of Pd sites on the catalyst surface [42,44].

Having identified the Pd/Fe_3O_4[wnf] system as the best catalyst in the CTH of BPE, we decided to evaluate its performance by investigating the effect of (i) the reaction temperature, (ii) the reaction time, and (iii) its stability in consecutive recycling tests.

Indeed, at lower temperature, the CTH of BPE showed a decrease in the conversion (20% at 210 °C and 5% at 180 °C, respectively) while the products distribution pattern remained unchanged within the investigated temperature range (Figure 7).

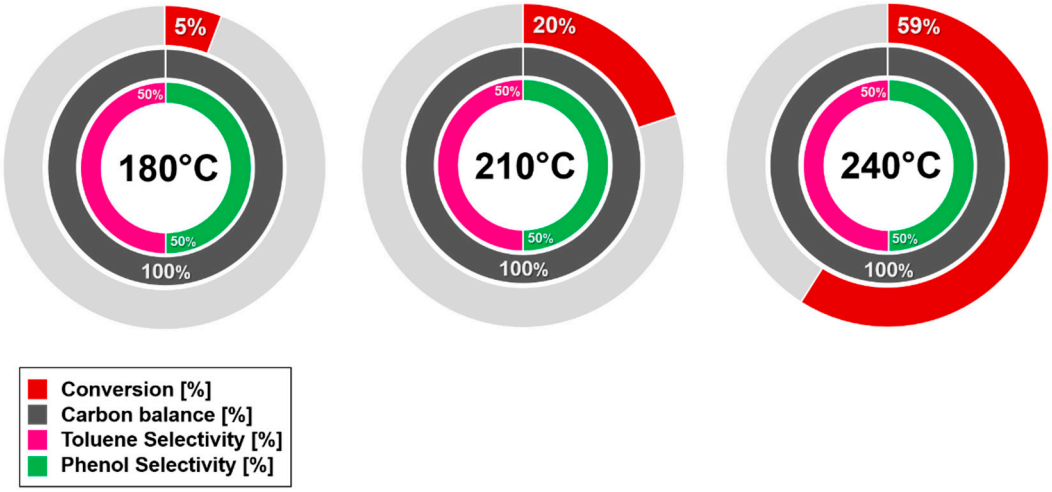

Figure 7. Reaction temperature effect in the catalytic transfer hydrogenolysis (CTH) of BPE in the presence of Pd/Fe_3O_4[wnf] catalyst and 2-propanol as solvent/H-source (reaction conditions: 0.125 g of catalyst; 40 mL of 0.1 M BPE solution; time, 90 min; N_2 pressure, 10 bar; stirring, 500 rpm).

The investigation of the CTH of BPE at 240 °C was also carried out at different reaction times (Figure 8). The BPE conversion was completed after 6 h, while a small presence of hydrogenated products (cyclohexanol) after 12h of reaction time was observed.

The stability and reusability of the Pd/Fe_3O_4[wnf] catalyst was also assessed at 240 °C (reaction time: 6 h). Pd/Fe_3O_4[wnf] maintained its high catalytic activity after six consecutive recycling runs and no changes in product selectivity were found (Figure 9). Furthermore, Pd/Fe_3O_4[wnf] could be magnetically recovered from reaction media and directly reused after being washed with 2-propanol.

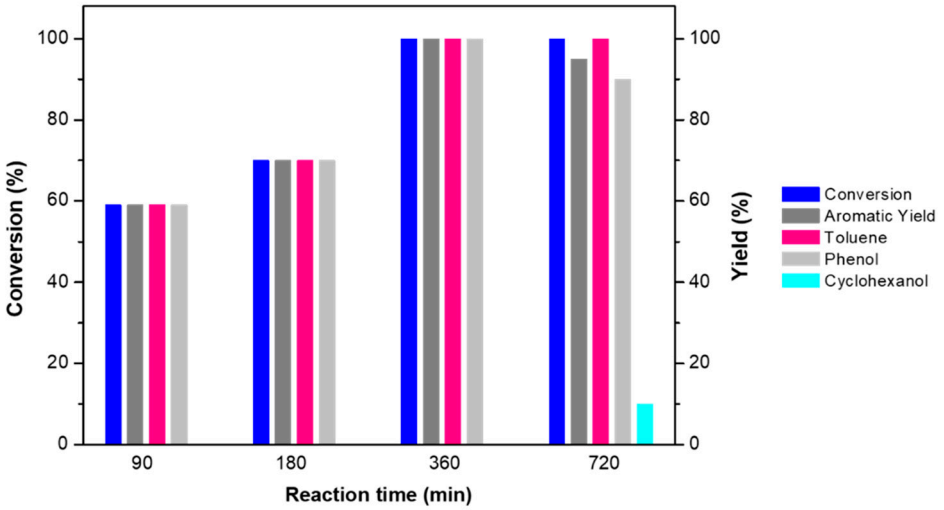

Figure 8. Reaction time effect in the CTH of BPE at 240 °C in the presence of Pd/Fe_3O_4[wnf] catalyst and 2-propanol as solvent/H-source (reaction conditions: 0.125 g of catalyst; 40 mL of 0.1 M BPE solution; temperature, 240 °C; N_2 pressure, 10 bar; stirring, 500 rpm).

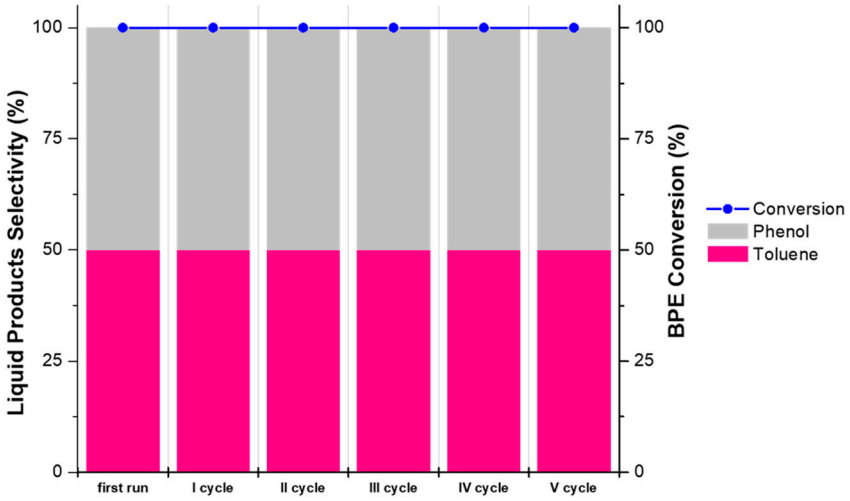

Figure 9. Recycling test of the Pd/Fe_3O_4[wnf] catalyst in the CTH of BPE at 240 °C (reaction conditions: 0.125 g of catalyst; 40 mL of 0.1 M BPE solution; time, 360 min; N_2 pressure, 10 bar; stirring, 500 rpm).

3. Materials and Methods

3.1. Catalyst Preparation

All chemicals were purchased from Carlo Erba Reagents (Italy), and used without additional purification. Before use, Pd/C was dried for 1 day under vacuum at 120 °C and finally reduced at 200 °C for 2 h under a hydrogen flow (1 cc/min).

The electrospinning apparatus consists of a syringe, a grounded collector, and a high-voltage power supply. In the spinning process, the syringe is filled with a polymer solution and a high voltage is applied between the syringe nozzle and the collector. The interaction between the charged polymer solution and the applied electric field provides the extrusion force. Many parameters such as applied voltage, solution feed rate, spinning distance, temperature, humidity, solution conductivity, and viscosity must be carefully adjusted in order to control morphology and properties of the electro-spun materials [17,45].

Two different approaches were explored for the synthesis of Pd-based iron oxide nanofibers: Pd/Fe_3O_4[wnf] and Pd/Fe_3O_4[cnf]. In the first case, the active metal was impregnated [46] onto the

nanofibrous support, whereas in the second one, the active metal was directly added in the spinnable solution, as depicted in Scheme 1. In detail, in the production of both the nanofibers, polyacrylonitrile (PAN), *N*,*N*-dimethylformamide (DMF), and iron(III) acetate were used as polymer, solvent, and iron source, respectively. At the same time, palladium(II) acetylacetonate was utilized as a palladium source. $FeAc_3$ (5.1 wt%) was mixed with DMF (90.6 wt%) and, once the solution was homogeneous, PAN (6.5 wt%) was dissolved and magnetically stirred for 4 h at room temperature. In the case of the sample Pd/Fe_3O_4[cnf], the palladium precursor (nominal palladium loading of 5%) was added to the spinnable solution together with the iron precursor (iron(III) acetate). Electrospinning of solutions was performed using the CH-01 Electro-spinner 2.0 (Linari Engineering s.r.l.) system, working at room temperature and at 40% of the relative humidity. A 10-cc glass syringe was equipped with a 20-mm-long stainless-steel needle with a diameter of 1 mm. Different working conditions were tested. Basically, the needle-to-collector distance was varied between 10 and 20 cm, the applied voltage ranged between 12 and 20 kV, and the feeding rate of the solution was tested between 0.95 and 2.02 mL/h. During the process, DMF evaporated very rapidly, and a membrane consisting of smooth nanofibers was finally obtained. Thereafter, in both cases, membranes were calcined in air at 600 °C for 2 h to eliminate the organic constituents of the fibers and to generate the iron oxide from its precursor, respectively named PdO/Fe_2O_3[wnf] and PdO/Fe_2O_3[cnf]. The so-called Pd/Fe_3O_4[wnf] and Pd/Fe_3O_4[cnf] catalysts were obtained after reduction in a standard apparatus at 200 °C for 2 h under flowing hydrogen (1 cc/min).

In the case of Pd/Fe_3O_4 catalyst, the wet impregnation of the commercial Fe_3O_4 powder with an acetone solution of palladium(II) acetylacetonate was performed. After impregnation, also in this case, the sample was dried for 1 day under vacuum at 120 °C and finally reduced at 250 °C for 2 h under a hydrogen flow (1 cc/min).

The main characteristics of the tested palladium-based catalysts are reported in Table 1.

3.2. Catalyst Characterization

SEM-EDX analyses were carried out on a Phenom Pro-X scanning electron microscope (SEM) equipped with an energy-dispersive X-ray spectrometer (EDX) in order to investigate the morphological features and elemental compositions of synthesized materials.

The mean diameter size of nanofibers was obtained by counting several hundred fibers visible on the micrographs of each sample. The EDX analysis was used to evaluate the metal loading and its dispersion over the support, acquiring, for all samples, at least 20 points for three different magnifications.

The phase composition of the fresh catalysts was analyzed by powder X-ray diffraction (XRD) using a Bruker D2 Phaser using Cu Kα radiation at 30 kV and 20 mA. The diffraction angles 2θ were varied between 10° and 80° in steps of 0.02° and a count time of 5 s per step. Peak attribution was performed on the basis of the JCPDS database of reference compounds.

Samples' thermal stability was evaluated by temperature-programmed TGA/DSC experiments with a Netzsch instrument. The temperature-programmed experiments were carried out in air in the range 25–550 °C with a heating rate of 10 °C/min.

The transmission electron microscopy (TEM) analysis was carried out using a JEOL 1400 Plus instrument operating at 120 kV, able to achieve a 0.19 nm point-to-point resolution and a 0.14 nm line resolution. Particle size distributions were obtained by counting several hundred particles visible on the micrographs of each sample.

The temperature-programmed reduction (H_2-TPR) was carried out with a Chemisorb Micromeritics 2750 instrument, to monitor the reduction of the metal oxides under a flux of 50 cm^3/min of H_2/Ar (10 vol.%) in the temperature range 25–1000 °C, at atmospheric pressure.

The Brunauer–Emmett–Teller (BET) surface areas of the prepared samples were determined from nitrogen adsorption–desorption isotherms at 77 K (ChemiSorb 2750 Micromeritics).

3.3. Catalytic Tests

Reactions were carried out in a 100-mL stainless-steel autoclave at a stirring speed of 500 rpm. The reactor containing the reduced catalyst (0.125 g) suspended in a 0.1 M solution of BPE in 2-propanol (40 mL), was purged several times with N_2 (99.99%) and successively pressurized at the desired N_2 pressure (10 bar), and finally heated at the necessary reaction temperature. At the end of every reaction, the system was cooled down and, when at room temperature, the pressure was carefully released, and the liquid phase was analyzed using an off-line gas chromatograph (Agilent 6890N equipped with CP-WAX 52CB, 60 m, i.d. 0.53 mm).

In all recycling tests, after any run, the catalyst was magnetically recovered, carefully washed with 2-propanol, and reused under the same reaction conditions.

The conversion, product selectivity, and yield in the liquid phase were calculated on the basis of the following equations:

$$\text{Conversion } [\%] = \frac{\text{mol of reacted BPE}}{\text{mol of BPE feed}} \times 100 \quad (1)$$

$$\text{Liquid phase selectivity } [\%] = \frac{\text{mol of specific product in liquid phase}}{\text{sum of mol of all products in liquid phase}} \times 100 \quad (2)$$

$$\text{Aromatic selectivity } [\%] = \frac{\text{mol of aromatic products in liquid phase}}{\text{mol of reaction products in liquid phase}} \times 100 \quad (3)$$

$$\text{Product Yield } [\%] = \frac{\text{mol of specific product}}{\text{mol of substrate feed}} \times 100 \quad (4)$$

4. Conclusions

The electrospinning technique was efficiently employed to prepare Pd-based catalysts on iron oxide to be used in the transfer hydrogenolysis reaction of benzyl phenyl ether.

Two synthetic procedures to obtain catalyst nanofibers were explored, highlighting the differences in the features of the produced nanofibers. The palladium co-electrospun with the iron support (Pd/Fe_3O_4[cnf]) was finely dispersed and embedded in the nanofibers of the support, whilst the Pd nanoparticles impregnated on nanofibers of the iron oxide support (Pd/Fe_3O_4[wnf]) were evenly dispersed and appeared firmly attached on the surface of the iron oxide nanofiber support. In both cases, palladium particles having nanometric dimension were detected.

The Pd/Fe_3O_4[wnf] catalyst was found to be efficient in the catalytic transfer hydrogenolysis of benzyl phenyl ether (α-O-4 lignin model molecule) producing phenol and toluene as the unique reaction products. Moreover, the Pd/Fe_3O_4[wnf] catalyst could be used up to six consecutive recycling runs without any significative loss in its catalytic performance, and was easily magnetically recoverable from the reaction medium. All these features make the Pd/Fe_3O_4[wnf] nanofibers a promising catalytic system in the reductive valorization of lignocellulosic biomasses.

Author Contributions: Conceptualization: A.M. (Angela Malara), E.P., L.B., F.M., A.M. (Anastasia Macario) and P.F.; Data curation: E.P.; Formal analysis: A.M. (Angela Malara), L.B., A.M. (Anastasia Macario), and P.F.; Funding acquisition: F.M.; Investigation: A.M. (Angela Malara), E.P., L.B., F.M., A.M. (Anastasia Macario), and P.F.; Supervision: A.M. (Angela Malara), E.P., L.B., F.M., A.M. (Anastasia Macario), and P.F.; Writing—original draft: A.M. (Angela Malara), E.P., L.B., F.M., A.M. (Anastasia Macario), and P.F.; Writing—review and editing: A.M. (Angela Malara), E.P., L.B., F.M., A.M. (Anastasia Macario), and P.F. All authors have read and agreed to the published version of the manuscript.

Funding: This publication was supported by the PON R&S 2014–2020 "e-Brewery—Virtualization, sensing and IoT for the innovation of beverage industrial production process" (code: ARS2017_0582).

Acknowledgments: The authors gratefully acknowledge the Centre for Microscopy and Microanalysis (CM2), Transmission Electron Microscopy Unit, Department of Biology, Ecology and Earth Science—University of Calabria, for TEM analyses. The authors thank Ing. Sofia Errigo for her precious help in catalysts preparation and for catalytic experiments related to the CTH of BPE. Authors acknowledge the networking contribution by the COST Action CA17128—Establishment of a Pan-European Network on the Sustainable Valorisation of Lignin.

Conflicts of Interest: The authors declare no conflict of interest.

References

1. Besson, M.; Gallezot, P.; Pinel, C. Conversion of biomass into chemicals over metal catalysts. *Chem. Rev.* **2014**, *114*, 1827–1870. [CrossRef]
2. Costilla, I.O.; Sanchez, M.D.; Gigola, C.E. Palladium nanoparticle's surface structure and morphology effect on the catalytic activity for dry reforming of methane. *Appl. Catal. A Gen.* **2014**, *478*, 38–44. [CrossRef]
3. Rezaei, M.; Meshkani, F.; Ravandi, A.B.; Nematollahi, B.; Ranjbar, A.; Hadian, N. Autothermal reforming of methane over Ni catalysts supported on nanocrystalline MgO with high surface area and plated-like shape. *Int. J. Hydrogen Energy* **2011**, *36*, 11712–11717. [CrossRef]
4. Lu, P.; Murray, S.; Zhu, M. Electrospun nanofibers for catalysts. In *Electrospinning: Nanofabrication and Applications*; Ding, B., Wang, X., Yu, J., Eds.; Micro and Nano Technologies Book Series; William Andrew: Norwich, NY, USA, 2019; pp. 695–717.
5. Wen, S.; Liang, M.; Zou, R.; Wang, Z.; Yue, D.; Liu, L. Electrospinning of palladium/silica nanofibers for catalyst applications. *RSC Adv.* **2015**, *5*, 41513–41519. [CrossRef]
6. Guo, L.P.; Bai, J.; Li, C.P.; Meng, Q.R.; Liang, H.O.; Sun, W.Y.; Li, H.Q.; Liu, H. A novel catalyst containing palladium nanoparticles supported on PVP composite nanofiber films: Synthesis, characterization and efficient catalysis. *Appl. Surf. Sci.* **2013**, *283*, 107–114. [CrossRef]
7. Bao, Y.; Luu, Q.A.N.; Zhao, Y.; Fong, H.; May, P.S.; Jiang, C. Upconversion polymeric nanofibers containing lanthanide-doped nanoparticles via electrospinning. *Nanoscale* **2012**, *4*, 7369–7375. [CrossRef]
8. Guan, A.H.Y.; Zhou, W.; Fu, S.W.; Shao, C.L.; Liu, Y.C. Electrospun nanofibers of NiO/SiO_2 composite. *J. Phys. Chem. Solids* **2009**, *70*, 1374–1377. [CrossRef]
9. Reneker, D.H.; Yarin, A.L. Electrospinning jets and polymer nanofibers. *Polymer* **2008**, *49*, 2387–2425. [CrossRef]
10. Frontera, P.; Candamano, S.; Macario, A.; Crea, F.; Scarpino, L.A.; Antonucci, P.L. Ferrierite zeolitic thin-layer on cordierite honeycomb support by clear solutions. *Mater. Lett.* **2013**, *104*, 72–75. [CrossRef]
11. Huang, Z.; Zhang, Y.; Kotaki, M.; Ramakrishna, S. A review on polymer nanofibers by electrospinning and their applications in nanocomposites. *Compos. Sci. Technol.* **2003**, *63*, 2223–2253. [CrossRef]
12. Varabhas, J.S.; Chase, G.G.; Reneker, D.H. Electrospun nanofibers from a porous hollow tube. *Polymer* **2008**, *49*, 4226–4229. [CrossRef]
13. Frenot, A.; Chronakis, I.S. Polymer nanofibers assembled by electrospinning. *Curr. Opin. Colloid Interface Sci.* **2003**, *8*, 64–67. [CrossRef]
14. Malara, A.; Frontera, P.; Bonaccorsi, L.; Antonucci, P.L. Hybrid zeolite SAPO-34 fibres made by electrospinning. *Materials* **2018**, *11*, 2555. [CrossRef] [PubMed]
15. Freni, A.; Calabrese, L.; Malara, A.; Frontera, P.; Bonaccorsi, L. Silica gel microfibres by electrospinning for adsorption chillers. *Energy* **2019**, *187*, 115971. [CrossRef]
16. Frontera, P.; Kumita, M.; Malara, A.; Nishizawa, J.; Bonaccorsi, L. Manufacturing and assessment of electrospun PVP/TEOS microfibres for adsorptive heat transformers. *Coatings* **2019**, *9*, 443. [CrossRef]
17. Fang, X.; Ma, H.; Xiao, S.L.; Shen, M.W.; Guo, R.; Cao, X.Y.; Shi, X.Y. Facile immobilization of gold nanoparticles into electrospun polyethyleneimine/polyvinyl alcohol nanofibers for catalytic applications. *J. Mater. Chem.* **2011**, *21*, 4493–4501. [CrossRef]
18. Thenmozhi, S.; Kadirvelu, K. Transfer hydrogenation and hydration of aromatic aldehydes and nitriles using heterogeneous NiO nanofibers as a catalyst. *New J. Chem.* **2018**, *42*, 15572–15577. [CrossRef]
19. Espro, C.; Gumina, B.; Paone, E.; Mauriello, F. Upgrading lignocellulosic biomasses: Hydrogenolysis of platform derived molecules promoted by heterogeneous Pd-Fe catalysts. *Catalysts* **2018**, *7*, 78. [CrossRef]
20. Gumina, B.; Mauriello, F.; Pietropaolo, R.; Galvagno, S.; Espro, C. Hydrogenolysis of sorbitol into valuable C3-C2 alcohols at low H_2 pressure promoted by the heterogeneous Pd/Fe_3O_4 catalyst. *Mol. Catal.* **2018**, *446*, 152–160. [CrossRef]
21. Cozzula, D.; Vinci, A.; Mauriello, F.; Pietropaolo, R.; Müller, T.E. Directing the cleavage of ester C−O bonds by controlling the hydrogen availability on the surface of coprecipitated Pd/Fe_3O_4. *ChemCatChem* **2016**, *8*, 1515–1522. [CrossRef]
22. Espro, C.; Gumina, B.; Szumelda, T.; Paone, E.; Mauriello, F. Catalytic transfer hydrogenolysis as an effective tool for the reductive upgrading of cellulose, hemicellulose, lignin, and their derived molecules. *Catalysts* **2018**, *8*, 313. [CrossRef]

23. Wang, D.; Astruc, D. The golden age of transfer hydrogenation. *Chem. Rev.* **2015**, *115*, 6621–6686. [CrossRef] [PubMed]
24. Tabanelli, T.; Paone, E.; Blair Vasquez, P.; Pietropaolo, R.; Cavani, F.; Mauriello, F. Transfer hydrogenation of methyl and ethyl levulinate promoted by a ZrO_2 catalyst: A comparison of batch vs. continuous gas-flow conditions. *ACS Sustain. Chem. Eng.* **2019**, *7*, 9937–9947. [CrossRef]
25. Paone, E.; Espro, C.; Pietropaolo, R.; Mauriello, F. Selective arene production from transfer hydrogenolysis of benzyl phenyl ether promoted by a co-precipitated Pd/Fe_3O_4 catalyst. *Catal. Sci. Technol.* **2016**, *6*, 7937–7941. [CrossRef]
26. Mauriello, F.; Paone, E.; Pietropaolo, R.; Balu, A.M.; Luque, R. Catalytic transfer hydrogenolysis of lignin-derived aromatic ethers promoted by bimetallic Pd/Ni systems. *ACS Sustain. Chem. Eng.* **2018**, *6*, 9269–9276. [CrossRef]
27. Mauriello, F.; Ariga-Miwa, H.; Paone, E.; Pietropaolo, R.; Takakusagi, S.; Asakura, K. Transfer hydrogenolysis of aromatic ethers promoted by the bimetallic Pd/Co catalyst. *Catal. Today* **2019**. [CrossRef]
28. Renders, T.; Van den Bosch, G.; Vangeel, T.; Van Aelst, K.; Sels, B. Reductive catalytic fractionation: State of the art of the lignin-first biorefinery. *Curr. Opin. Biotechnol.* **2019**, *56*, 193–201. [CrossRef]
29. Paone, E.; Tabanelli, T.; Mauriello, F. The rise of lignin biorefinery. *Curr. Opin. Green Sustain. Chem.* **2019**. [CrossRef]
30. Schutyser, W.; Renders, T.; Van den Bosch, S.; Koelewijn, S.F.; Beckham, G.T.; Sels, B.T. Chemicals from lignin: An interplay of lignocellulose fractionation, depolymerisation, and upgrading. *Chem. Soc. Rev.* **2018**, *47*, 852–908. [CrossRef]
31. Sun, Z.; Fridrich, B.; de Santi, A.; Elangovan, S.; Barta, K. Bright side of lignin depolymerization: Toward new platform chemicals. *Chem. Rev.* **2018**, *118*, 614–678. [CrossRef]
32. Galkin, M.V.; Samec, J.S.M. Lignin valorization through catalytic lignocellulose fractionation: A fundamental platform for the future biorefinery. *ChemSusChem* **2016**, *9*, 1544–1558. [CrossRef] [PubMed]
33. Renders, T.; Van den Bosch, S.; Vangeel, T.; Ennaert, T.; Koelewijn, S.F.; Van den Bossche, G.; Courtin, C.M.; Schutyser, W.; Sels, B.F. Synergetic effects of alcohol/water mixing on the catalytic reductive fractionation of poplar wood. *ACS Sustain. Chem. Eng.* **2016**, *4*, 6894–6904. [CrossRef]
34. Galkin, M.V.; Samec, J.S.M. Selective route to 2-propenyl aryls directly from wood by a tandem organosolv and palladium-catalysed transfer hydrogenolysis. *ChemSusChem* **2014**, *7*, 2154–2158. [CrossRef] [PubMed]
35. Yan, N.; Zhao, C.; Dyson, P.J.; Wang, C.; Liu, L.-T.; Kou, Y. Selective degradation of wood lignin over noble-metal catalysts in a two-step process. *ChemSusChem* **2008**, *1*, 626–629. [CrossRef]
36. Song, S.; Zhang, J.; Gözaydın, G.; Yan, N. Production of terephthalic acid from corn stover lignin. *Angew. Chem.* **2019**, *58*, 4934–4937. [CrossRef]
37. Torr, K.M.; van de Pas, D.J.; Cazeils, E.; Suckling, I.D. Mild hydrogenolysis of in-situ and isolated *Pinus radiata* lignins. *Bioresour. Technol.* **2011**, *102*, 7608–7611. [CrossRef]
38. Xue, T.J.; McKinney, M.A.; Wilkie, C.A. The thermal degradation of polyacrylonitrile. *Polym. Degrad. Stab.* **1997**, *58*, 193–202. [CrossRef]
39. Sexton, B.A.; Hughes, A.E.; Turney, T.W. An XPS and TPR study of the reduction of promoted cobalt-kieselguhr Fischer-Tropsch catalysts. *J. Catal.* **1986**, *97*, 390–406. [CrossRef]
40. Ji, Y.; Zhao, Z.; Duan, A.; Jiang, G.; Jian, L. Comparative study on the formation and reduction of bulk and Al_2O_3-supported cobalt oxides by H_2-TPR technique. *J. Phys. Chem. C* **2009**, *113*, 7186–7199. [CrossRef]
41. Zhou, H.; Song, J.; Fan, H.; Zhang, B.; Yang, Y.; Hu, J.; Zhua, Q.; Han, B. Cobalt catalysts: Very efficient for hydrogenation of biomass-derived ethyl levulinate to gamma-valerolactone under mild conditions. *Green Chem.* **2014**, *16*, 3870–3875. [CrossRef]
42. Liu, L.; Corma, A. Metal catalysts for heterogeneous catalysis: From single atoms to nanoclusters and nanoparticles. *Chem. Rev.* **2018**, *118*, 4981–5079. [CrossRef] [PubMed]
43. Mauriello, F.; Armandi, M.; Bonelli, B.; Onida, B.; Garrone, E. H-bonding of furan and its hydrogenated derivatives with the isolated hydroxyl of amorphous silica: An IR spectroscopic and thermodynamic study. *J. Phys. Chem. C* **2010**, *114*, 18233–18239. [CrossRef]
44. De Rogatis, L.; Cargnello, M.; Gombac, V.; Lorenzut, B.; Montini, T.; Fornasiero, P. Embedded phases: A way to active and stable catalysts. *ChemSusChem* **2010**, *3*, 24–42. [CrossRef] [PubMed]

45. Frontera, P.; Malara, A.; Stelitano, S.; Fazio, E.; Neri, F.; Scarpino, L.; Antonucci, P.L.; Santangelo, S. A new approach to the synthesis of titania nano-powders enriched with very high contents of carbon nanotubes by electro-spinning. *Mater. Chem. Phys.* **2015**, *153*, 338–345. [CrossRef]
46. Frontera, P.; Macario, A.; Malara, A.; Antonucci, V.; Modafferi, V.; Antonucci, P.L. Simultaneous methanation of carbon oxides on nickel-iron catalysts supported on ceria-doped gadolinia. *Catal. Today* **2019**. [CrossRef]